Colloid Polym Sci 276:459–469 (1998)

ORIGINAL CONTRIBUTION

D.Y. Kwok
A. Leung
A. Li
C.N.C. Lam
R. Wu
A.W. Neumann

Low-rate dynamic contact angles on poly(*n*-butyl methacrylate) and the determination of solid surface tensions

Received: 12 September 1997
Accepted: 22 January 1998

This paper represents, in part, the Ph.D. thesis of D.Y. Kwok

D.Y. Kwok · A. Leung · A. Li · C.N.C. Lam
R. Wu · A.W. Neumann (✉)
Department of Mechanical and Industrial Engineering
University of Toronto
5 Kings's College Road
Toronto, Ontario M5S 3G8
Canada
E-mail: neumann@mie.utoronto.ca

Abstract Low-rate dynamic contact angles of 22 liquids on a poly(*n*-butyl methacrylate) (P*n*BMA) polymer are measured by an automated axi-symmetric drop shape analysis-profile (ADSA-P). It is found that 16 liquids yielded non-constant contact angles, and/or dissolved the polymer on contact. From the experimental contact angles of the remaining 6 liquids, it is found that the liquid–vapor surface tension times cosine of the contact angle changes smoothly with the liquid–vapor surface tension, i.e. $\gamma_{lv}\cos\theta$ depends only on γ_{lv} for a given solid surface (or solid surface tension). This contact angle pattern is in harmony with those from other inert and non-inert (polar and non-polar) surfaces [34–37, 45–47]. The solid–vapor surface tension calculated from the equation-of-state approach for solid-liquid interfacial tensions [14] is found to be 28.8 mJ/m^2, with a 95% confidence limit of $\pm$0.5 mJ/m^2, from the experimental contact angles of the 6 liquids.

Key words Poly(*n*-butyl methacrylate)-polymer – contact angle – surface tension

Introduction

Several independent approaches have been used to estimate solid surface tensions, including direct force measurements [1–9], contact angles [10–17], capillary penetration into columns of particle powder [18–21], sedimentation of particles [22–25], solidification fronts of particles [26, 27], gradient theory [28], and Lifshitz theory of van der Waals forces [28, 29]. Among these methods, contact angle measurement is believed to be the simplest approach for surface energetics.

At the centre of contact angle research is Young's equation,

$$\gamma_{lv}\cos\theta_Y = \gamma_{sv} - \gamma_{sl} \quad (1)$$

which interrelates the Young contact angle with the interfacial tensions of the liquid–vapor γ_{lv}, solid–vapor γ_{sv}, and solid–liquid γ_{sl} interfaces; θ_Y is the Young contact angle, i.e. a contact angle which can be used in conjunction with Young's equation. While there are a number of thermodynamic equilibrium contact angles θ_e, they are not necessarily equal to θ_Y in Young's equation [30–32]:

(1) On ideal solid surfaces, there is no contact angle hysteresis and the experimentally observed contact angle is equal to θ_Y.

(2) On smooth, but chemically heterogeneous solid surfaces, θ is not necessarily equal to the thermodynamic equilibrium angle. Nevertheless, the experimental advancing contact angle, θ_a, can be expected to be a good approximation of θ_Y. Therefore, care must be exercised to ensure that the experimental apparent contact angle, θ, is the advancing contact angle to be inserted into the Young equation.

(3) On rough solid surfaces, no such equality between advancing contact angle and θ_Y exists. Thus, contact angles measured on rough surfaces cannot be used in conjunction with Young's equation.

Although the Wenzel and Cassie angles represent the thermodynamic equilibrium angles on rough and heterogeneous surfaces, respectively, they are not equal to θ_Y. Equation (1) implies a single, unique contact angle; in practice, however, contact angle phenomena are complicated [30–32]. For example, the contact angle made by an advancing liquid (θ_a) and that made by a receding liquid (θ_r) are not identical; nearly all solid surfaces exhibit contact angle hysteresis, H (the difference between θ_a and θ_r):

$$H = \theta_a - \theta_r \,. \tag{2}$$

Contact angle hysteresis can be due to roughness and heterogeneity of a solid surface. If roughness is the primary cause, then the measured contact angles are meaningless in terms of Young's equation. On rough surfaces, advancing contact angles are larger than on chemically identical smooth surfaces [21] which do not reflect material properties of the surface, rather they reflect morphological ones.

Recently, we have shown [33–37] that measuring contact angles at very slow motion of the three-phase contact line allows direct observation of surface quality. In addition, when such procedures are interpreted by an automated axisymmetric drop shape analysis-profile (ADSA-P), complexities such as dissolution of the polymer by the liquid and slip/stick of the three-phase contact line, which affect the contact angle interpretation in terms of surface energetics, can be identified [35–37].

In this study, we report low-rate dynamic contact angles of various liquids on a poly(*n*-butyl methacrylate) (P*n*BMA) polymer by ADSA-P. The P*n*BMA-coated surface is prepared by a solvent-casting technique; surface roughness is in the order of nanometers or less. These dynamic (advancing) contact angles are then employed for the interpretation in terms of solid surface tensions.

Materials (solid surface and liquids)

Poly(*n*-butyl methacrylate) (P*n*BMA) was purchased from Polysciences (Warrington, P.A.; cat # 02061) as a fine powder. A 2% P*n*BMA/chloroform solution was prepared using chloroform (Sigma-Aldrich, 99.9 + % A.C.C. HPLC grade) as the solvent. Silicon wafers ⟨1 0 0⟩ (Silicon Sense, Naschua, N.H.; thickness: 525 ± 50 micron) were selected as the substrate for polymer coating. They were obtained as circular discs of about 10 cm diameter and were cut into rectangular shapes of about 2.5 cm × 5 cm. Each rectangular wafer surface was then soaked in chromic acid for at least 24 h, rinsed with doubly distilled water, and dried under a heat lamp before polymer coating.

The P*n*BMA-coated surfaces were prepared by a solvent-casting technique: a few drops of the 2% P*n*BMA/chloroform solution were deposited on dried silicon wafers inside glass dishes overnight; the solution spreads and a thin layer of the P*n*BMA formed on the wafer surface after chloroform evaporation. This preparation produced coated surfaces good quality, as manifested by light fringes, due to refraction at these surfaces, suggesting that surface roughness is in the order of nanometers or less.

With respect to the low-rate dynamic contact angle measurements by ADSA-P, liquid was supplied to the sessile drop from below the wafer surfaces using a motorized syringe device [35–37]. In order to facilitate such an experimental procedure, a hole of about 1 mm diameter was made, by using a diamond drill bit from Lunzer (New York, NY; SMS-0.027), in the center of each rectangular wafer surface before soaking in chromic acid. This strategy was pioneered by Oliver et al. [38, 39] to measure sessile drop contact angles because of its potential for avoiding drop vibrations and for measuring true advancing contact angles without disturbing the drop profile. In order to avoid leakage between a stainless steel needle (Chromatographic Specialities, Brockville, Ont; N723 needles pt. # 3, H91023) and the hole (on the wafer surface), Teflon tape was wrapped around the end of the needle before insertion into the hole. In the literature, it is customary to first deposit a drop of liquid on a given solid surface using a syringe or a Teflon needle; the drop is then made to advance by supplying more liquid from above using a syringe or a needle in contact with the drop. Such experimental procedures cannot be used for ADSA-P since ADSA determines the contact angles and surface tensions based on a complete and undisturbed drop profile.

Twenty two liquids were chosen in this study. Selection of these liquids was based on the following criteria: (1) they should include a wide range of intermolecular forces; (2) they should be non-toxic; and (3) the liquid surface tension should be higher than the anticipated solid surface tension [10, 14, 21]. They are listed in Table 1, together with the physical properties and surface tensions (measured at 23.0 ± 0.5 °C).

Methods and procedures

ADSA-P is a technique to determine liquid–fluid interfacial tensions and contact angles from the shape of axisymmetric menisci, i.e., from sessile as well as pendant drops [40]. Assuming that the experimental drop is Laplacian and axisymmetric, ADSA-P finds a theoretical profile that best matches the drop profile extracted from an image of a real drop, from which the surface tension, contact angle, drop volume, surface area and three-phase contact radius can be computed. The strategy employed is to fit the shape of an experimental drop to a theoretical

Table 1 Supplier, purity and surface tension of the liquids used

Liquid	Supplier	% Purity	Density [g/cm^3]	γ_{lv} [mJ/m^2]	No. of drops
cis-Decalin	Aldrich	99	0.897	32.32 ± 0.01	7
Nitromethane	Aldrich	99+	1.127	34.31 ± 0.006	10
2,5-Dichlorotoluene	Aldrich	98	1.254	34.64 ± 0.003	10
Triacetin	Fluka	99+	1.158	35.52 ± 0.16	10
Ethyl cyanoacetate	Aldrich	98+	1.063	36.01 ± 0.04	9
N,*N*-Dimethylformamide	Sigma-aldrich	99.9+ (HPLC)	0.944	36.65 ± 0.004	10
Ethyl cinnamate	Aldrich	99	1.049	37.17 ± 0.02	10
Methyl salicylate	Aldrich	99+	1.174	38.82 ± 0.07	10
Dibenzylamine	Aldrich	97	1.026	40.80 ± 0.06	9
Dimethyl sulfoxide (DMSO)	Sigma-aldrich	99.9 (HPLC)	1.101	42.68 ± 0.03	7
1-Iodonaphthalene	Aldrich	99	1.740	42.92 ± 0.03	10
1-Bromonaphthalene	Aldrich	98	1.489	44.31 ± 0.05	7
Diethylene glycol	Aldrich	99	1.118	44.68 ± 0.03	9
1,3-Diiodopropane	Aldrich	99	2.576	46.51 ± 0.13	10
3-Pyridylcarbinol	Aldrich	98	1.124	47.81 ± 0.03	10
Ethylene glycol	Aldrich	99+	1.113	48.66 ± 0.06	10
1,1,2,2-Tetrabromoethane	Aldrich	98	2.967	49.29 ± 0.05	10
Diiodomethane	Aldrich	99	3.325	49.98 ± 0.02	10
2,2′-Thiodiethanol	Aldrich	99+	1.221	53.77 ± 0.03	10
Formamide	Aldrich	99.5+	1.134	59.08 ± 0.04	10
Glycerol	Baker analyzed	99.8	1.258	65.02 ± 0.04	8
Water	LAST[1)]	Doubly distilled	0.977	72.70 ± 0.09	10

[1)] Laboratory of applied surface thermodynamics.

drop profile according to the Laplace equation of capillarity, using surface/interfacial tension as an adjustable parameter. The best fit identifies the correct surface/interfacial tension from which the contact angle can be determined by a numerical integration of the Laplace equation. Details of the methodology and experimental set-up can be found elsewhere [35–37, 40–42].

Sessile drop experiments were performed by ADSA-P to determine contact angles. The temperature and relative humidity were maintained, respectively, at 23.0 ± 0.5 °C and at about 40%. It has been found that, since ADSA assumes an axisymmetric drop shape, the values of liquid surface tensions measured from sessile drops are very sensitive to even a very small amount of surface imperfection, such as roughness and heterogeneity, while contact angles are less sensitive. Therefore, the liquid surface tensions used in this study were independently measured by applying ADSA-P to a pendant drop, since the axisymmetry of the drop is enforced by using a circular capillary. Results of the liquid surface tension are given in Table 1.

In this study, 6 dynamic contact angle measurements at velocities of the three-phase contact line in the range from 0.1 to 1.2 mm/min were performed for each liquid. The choice of this velocity range was based on previous studies [33–37] which showed that low-rate dynamic contact angles at these velocities are essentially identical to the static contact angles, for these relatively smooth surfaces.

In actual experiments, an initial liquid drop of about 0.3 cm radius was carefully deposited, covering the hole on the surface. This is to ensure that the drop will increase axisymmetrically in the center of the image field when liquid is supplied from the bottom of the surface and will not hinge on the lip of the hole. The motor in the motorized syringe mechanism was then set to a specific speed, by adjusting the voltage from a voltage controller. Such a syringe mechanism pushes the syringe plunger, leading to an increase in drop volume and hence the three-phase contact radius. A sequence of pictures of the growing drop was then recorded by the computer typically at a rate of 1 picture every 2–5 s, until the three-phase contact radius was about 0.5 cm or larger. For each low-rate dynamic contact angle experiment, at least 50 and up to 200 images were normally taken. Since ADSA-P determines the contact angle and the three-phase contact radius simultaneously for each image, the advancing dynamic contact angles as a function of the three-phase contact radius (i.e. location on the surface) can be obtained. The actual rate of advancing can be determined by linear regression, by plotting the three-phase contact radius over time. For each liquid, different rates of advancing were studied, by adjusting the speed of the pumping mechanism.

It should be noted that measuring contact angles as a function of the three-phase contact radius has an additional advantage: the quality of the surface is observed indirectly in the measured contact angles. If a solid surface

is not very smooth, irregular and inconsistent contact angle values will be seen as a function of the three-phase contact radius. When the measured contact angles are essentially constant at different surface locations, the mean contact angle for a specific rate of advancing can be obtained by averaging the contact angles, after the three-phase contact radius reaches 0.3 to 0.5 cm (see later). The purpose of choosing these relatively large drops is to avoid any line tension effects on the measured contact angles [43, 44]; it has been found that line tensions have very little effect on the measured contact angles in this range.

Results and discussion

Of the 22 liquids used, it was found that only 6 liquids yielded usable contact angles. They are water, glycerol, formamide, 2,2′-thiodiethanol, 3-pyridylcarbinol, and diethylene glycol. The rest of the 16 liquids either dissolved the polymer on contact or yielded non-constant contact angles during the course of the experiments.

Figures 1a–f show, respectively, typical experimental results of water, glycerol, formamide, 2,2′-thiodiethanol, 3-pyridylcarbinol, and diethylene glycol: all contact angles are essentially constant, as the drop volume V increases and hence the three-phase contact radius R. Increasing the drop volume in this manner ensures the measured θ to be an advancing contact angle. In all these cases, the measured contact angles are essentially constant as R increases. This indicates good surface quality of the surfaces used. It turns out that averaging the measured contact angles after R reaches 0.35 cm is convenient, since the drop is guaranteed to be in the advancing mode and that line tension effects are negligible. While this may seem to be an arbitrary value, it turns out that there is virtually no dependence on the choice of the starting point. In Fig. 1d, the contact line of 2,2′-thiodiethanol appears to stick on the surface at the beginning of the experiment, but not once the drop has started advancing. This suggests that 2,2′-thiodiethanol has a tendency to stick on the surface.

It should be noted that the liquid–vapor surface tension values calculated by ADSA-P sessile drop are fairly constant, but not as reliable as those from pendant drop. The accuracy relies very much on the axisymmetry of the drop profile. This can be seen in Fig. 1d, where the drop front sticks and moves, so that the axisymmetry of the drop profile is disturbed, resulting in a slight discontinuity of the apparent γ_{lv} values.

The remaining 16 liquids all show very complex contact angle behavior, as given in Figs. 2a–p. Figure 2a shows the contact angle results of diiodomethane. It can be seen that initially the apparent drop volume, as perceived by ADSA-P, increases linearly, and θ increases from 55° to 95° at essentially constant R. Suddenly, the drop front jumps to a new location as more liquid is supplied into the sessile drop. The resulting θ decreases sharply from 95° to 45°. As more liquid is supplied into the sessile drop, the contact angle increases again. Such slip/stick behavior could be due to non-inertness of the surface. Phenomenologically, an energy barrier for the drop front exists, resulting in sticking, which causes θ to increase at constant R. However, as more liquid is supplied into the sessile drop, the drop front possesses enough energy to overcome the energy barrier, resulting in slipping, which causes θ to decrease suddenly. It should be noted that as the drop front jumps from one location to the next, it is unlikely that the drop is or will remain axisymmetric. Such a non-axisymmetric drop will obviously not meet the basic assumptions underlying ADSA-P, causing possible errors, e.g., in the apparent surface tension and drop volume. This can be seen from the discontinuity of the apparent surface tension and drop volume with time as the drop front sticks and slips. Obviously, the observed angles in Fig. 2a cannot all be the Young contact angles; since γ_{lv}, γ_{sv}, (and γ_{sl}) are constants, θ ought to be a constant because of Young's equation. In addition, it is difficult to decide unambiguously at this moment whether or not Young's equation is applicable at all because of lack of understanding of the slip/stick mechanism. Therefore, these contact angles should not be used for the interpretation in terms of surface energetics.

Yet another contact angle pattern can be seen in Fig. 2b for 1,1,2,2-tetrabromoethane: θ increases at the beginning and decreases as the experiment proceeded, with γ_{lv} decreasing from that of the pure liquid. This suggests that dissolution of P*n*BMA by the liquid occurs. A different contact angle behavior again is given in Fig. 2c: the contact angle of ethylene glycol increases as R increases, suggesting that a physico-chemical reaction takes place at the solid–liquid interface during the experiment. Obviously, these angles should be disregarded for the following reasons: (1) γ_{lv} is different from that of the pure liquids; (2) we are unsure whether or not γ_{sl} and γ_{sv} remain constant and whether Young's equation is applicable.

There is yet another contact angle pattern which we wish to address: the patterns shown in Figs. 2f, j and p are very interesting. They can be thought of as a combination of a slip/stick pattern and the patterns shown in Figs. 2c and e. In these figures, the contact angle increases nonlinearly and R increases slowly; suddenly the drop front slips to a new location and the contact angle increases again in a similar manner; the reason for this pattern is unknown, and, for our purposes, irrelevant. These angles should not be used for the interpretation in terms of surface energetics, for reasons discussed earlier.

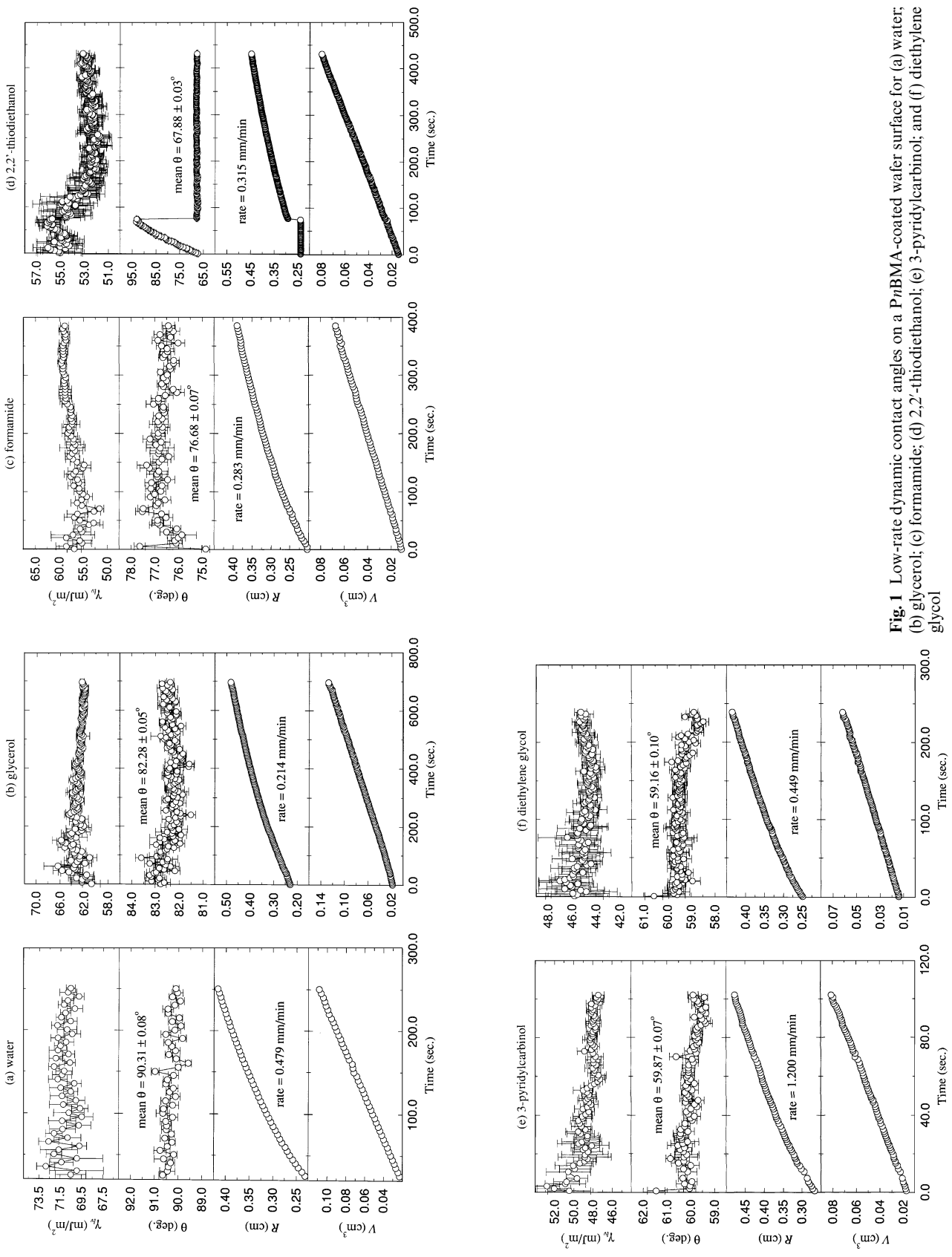

Fig. 1 Low-rate dynamic contact angles on a P*n*BMA-coated wafer surface for (a) water; (b) glycerol; (c) formamide; (d) 2,2'-thiodiethanol; (e) 3-pyridylcarbinol; and (f) diethylene glycol

Colloid & Polymer Science, Vol. 276, No. 6 (1998)

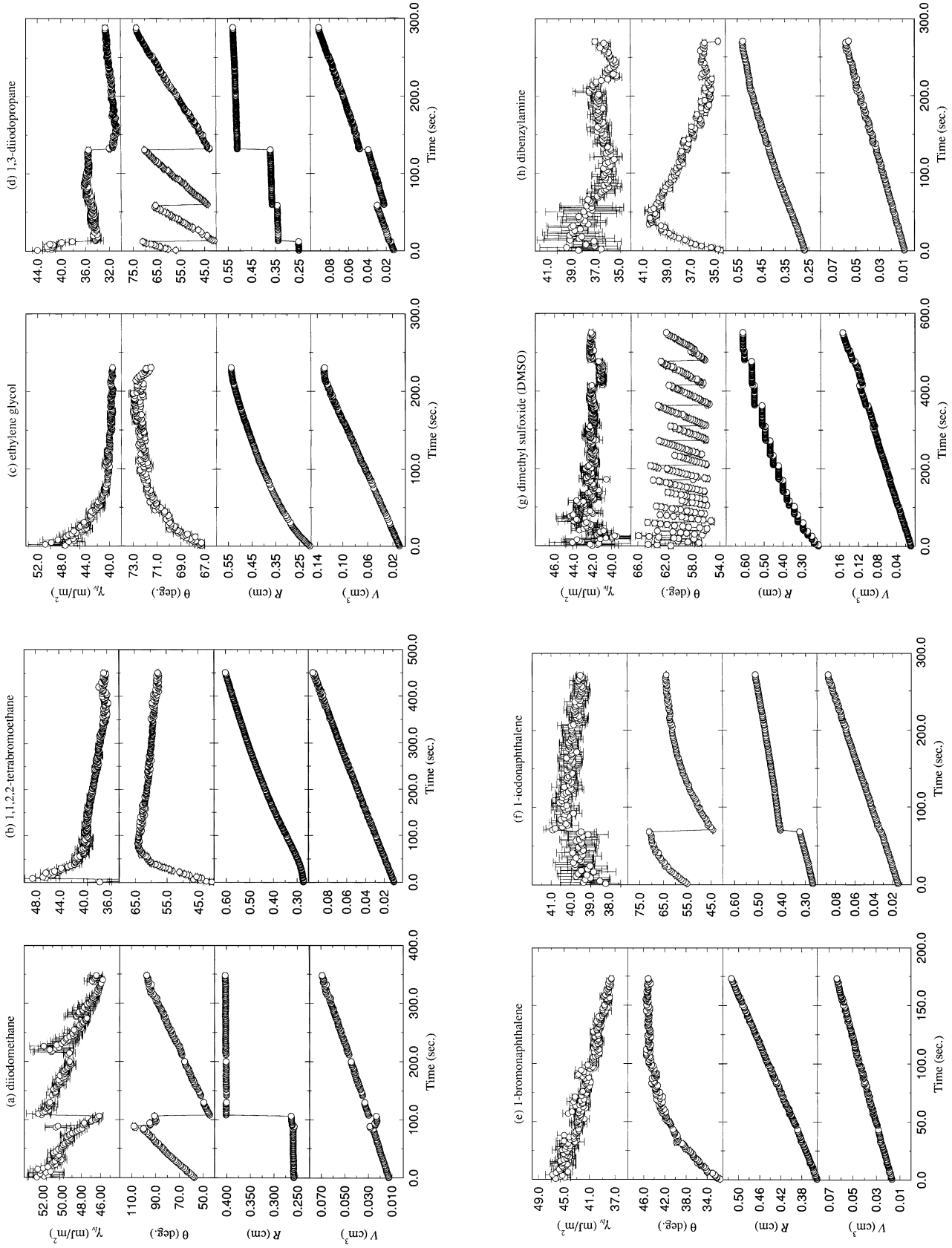

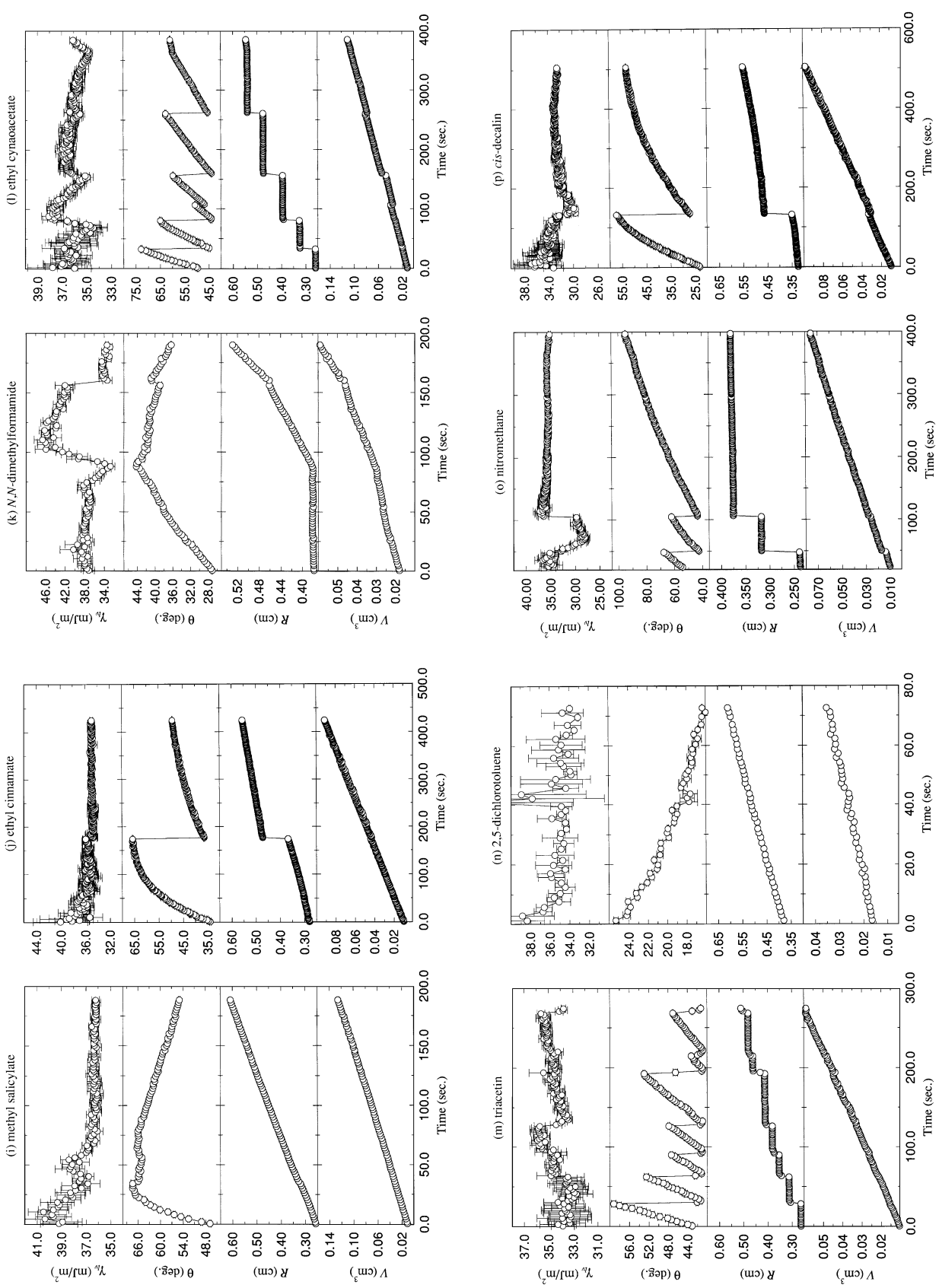

Fig. 2 Low-rate dynamic contact angles on a P*n*BMA-coated wafer surface for (a) diiodomethane; (b) 1,1,2,2-tetrabromoethane; (c) ethylene glycol; (d) 1,3-diiodopropane; (e) 1-bromonaphthalene; (f) 1-iodonaphthalene; (g) dimethyl sulfoxide (DMSO); (h) dibenzylamine; (i) methyl salicylate; (j) ethyl cinnamate; (k) *N*,*N*-dimethylformamide; (l) ethyl cyanoacetate; (m) triacetin; (n) 2,5-dichlorotoluene; (o) nitromethane; (p) *cis*-decalin. These angles cannot be used for the interpretation in terms of surface energetics, see text

The reproducibility of all solid–liquid systems is excellent. They are summarized in Table 2 for the 6 liquids with usable contact angles, at different rates of advancing and each on a newly prepared surface. It should be noted that a total of more than 130 freshly prepared P*n*BMA-coated wafers were prepared and used; more than 10 000 images were acquired and analyzed by ADSA-P. In the specific case of water in Table 2, a final value of $\theta = 90.73^\circ \pm 0.79^\circ$ was obtained, by averaging the contact angles from different rates of advancing (for different experiments). The 95% confidence limits calculated in this manner (in Table 2) include all possible errors, due to experimental technique, solid surface preparation, etc. A summary of the contact angle complexities is given in Table 3, together with the meaningful results from Table 2.

Disregarding the inconclusive contact angle data in Fig. 2, we show in Fig. 3 the contact angle results from Table 2, by plotting $\gamma_{lv}\cos\theta$ vs. γ_{lv}. It can be seen that all liquids independent of molecular properties fall on a smooth curve, in agreement with the patterns obtained in previous studies [34–37, 45–47]: the values of $\gamma_{lv}\cos\theta$ change smoothly with γ_{lv}, so that we again conclude that

$$\gamma_{lv}\cos\theta = F(\gamma_{lv}, \gamma_{sv}) \tag{3}$$

and hence, because of Young's equation

$$\gamma_{sl} = f(\gamma_{lv}, \gamma_{sv})\,. \tag{4}$$

Thus, the surface tension component approaches [11, 15–17] clash directly with these experimental results: the surface tension component approaches [11, 15–17]

Table 2 Summary of the advancing contact angles (deg.) at different rates (mm/min.) of motion of the three-phase contact line for liquids which yielded constant contact angles on a poly(*n*-butyl methacrylate) (P*n*BMA)-coated silicon wafer

Water		Glycerol		Formamide		2,2′-Thiodiethanol		3-Pyridylcarbinol		Diethylene glycol	
Rate	θ	Rate	θ	Rate	θ	Rate	θ	Rate	θ	Rate	θ
0.130	91.66 ± 0.35	0.214	82.28 ± 0.05	0.214	76.65 ± 0.04	0.229	68.01 ± 0.03	0.344	60.35 ± 0.15	0.332	59.14 ± 0.08
0.131	91.70 ± 0.35	0.218	82.13 ± 0.05	0.223	75.86 ± 0.04	0.238	68.12 ± 0.05	0.578	60.35 ± 0.07	0.380	58.97 ± 0.09
0.164	90.42 ± 0.23	0.223	82.28 ± 0.03	0.239	76.86 ± 0.06	0.284	68.33 ± 0.06	0.609	60.23 ± 0.15	0.381	58.76 ± 0.14
0.225	90.39 ± 0.12	0.224	81.87 ± 0.08	0.254	76.97 ± 0.07	0.315	67.88 ± 0.03	0.681	60.59 ± 0.18	0.449	59.16 ± 0.04
0.358	89.92 ± 0.12	0.230	82.23 ± 0.07	0.266	75.43 ± 0.05	0.427	67.98 ± 0.07	0.858	60.40 ± 0.09	0.451	58.83 ± 0.03
0.479	90.31 ± 0.08	0.251	81.96 ± 0.05	0.283	76.68 ± 0.07	0.643	67.69 ± 0.08	1.200	59.87 ± 0.07	0.503	57.52 ± 0.16
	90.73 ± 0.79[1)]		82.11 ± 0.21[1)]		76.41 ± 0.65[1)]		68.00 ± 0.23[1)]		60.30 ± 0.25[1)]		58.73 ± 0.64[1)]

[1)] Mean θ value with the 95% confidence limits.

Table 3 Summary of contact angle results for a poly(*n*-butyl methacrylate) (P*n*BMA)-coated silicon wafer surface

Liquids	γ_{lv} [mJ/m^2]	θ [deg.]
cis-Decalin	32.32	$\theta\uparrow$ as $R\uparrow$ (and slips) ($25^\circ \rightarrow 55^\circ$)
Nitromethane	34.31	slip/stick ($40^\circ \rightarrow 95^\circ$)
2,5-Dichlorotoluene	34.64	$\theta\downarrow$ as $R\uparrow$ ($26^\circ \rightarrow 16^\circ$) [1)]
Triacetin	35.53	slip/stick ($40^\circ \rightarrow 54^\circ$)
Ethyl cyanoacetate	36.01	slip/stick ($45^\circ \rightarrow 65^\circ$)
N,*N*-Dimethylformamide	36.65	$\theta\downarrow$ as $R\uparrow$ ($44^\circ \rightarrow 36^\circ$) [1)]
Ethyl cinnamate	37.17	$\theta\uparrow$ as $R\uparrow$ (and slips) ($35^\circ \rightarrow 65^\circ$)
Methyl salicylate	38.82	$\theta\uparrow\downarrow$ as $R\uparrow$ ($45^\circ \rightarrow 66^\circ \rightarrow 54^\circ$)
Dibenzylamine	40.80	$\theta\uparrow\downarrow$ & $\gamma_{lv}\downarrow$ as $R\uparrow$ ($32^\circ \rightarrow 41^\circ \rightarrow 38^\circ$)
Dimethyl sulfoxide (DMSO)	42.68	slip/stick ($56^\circ \rightarrow 64^\circ$)
1-Iodonaphthalene	42.92	$\theta\uparrow$ as $R\uparrow$ (and slips) ($45^\circ \rightarrow 65^\circ$)
1-Bromonaphthalene	44.31	$\theta\uparrow$ & $\gamma_{lv}\downarrow$ as $R\uparrow$ ($32^\circ \rightarrow 46^\circ$)
Diethylene glycol	45.16	58.73 ± 0.64
1,3-Diiodopropane	46.51	slip/stick ($40^\circ \rightarrow 75^\circ$)
Ethylene glycol	47.55	$\theta\uparrow$ & $\gamma_{lv}\downarrow$ as $R\uparrow$ ($67^\circ \rightarrow 73^\circ$)
3-Pyridylcarbinol	47.81	60.30 ± 0.25
1,1,2,2-Tetrabromoethane	49.29	$\theta\uparrow\downarrow$ & $\gamma_{lv}\downarrow$ as $R\uparrow$ ($40^\circ \rightarrow 65^\circ \rightarrow 56^\circ$)
Diiodomethane	49.98	slip/stick ($60^\circ \rightarrow 100^\circ$)
2,2′-Thiodiethanol	53.77	68.00 ± 0.23
Formamide	59.08	76.41 ± 0.65
Glycerol	65.02	82.11 ± 0.21
Water	72.70	90.73 ± 0.79

[1)] Part of the polymer was observed to be removed after the experiment.

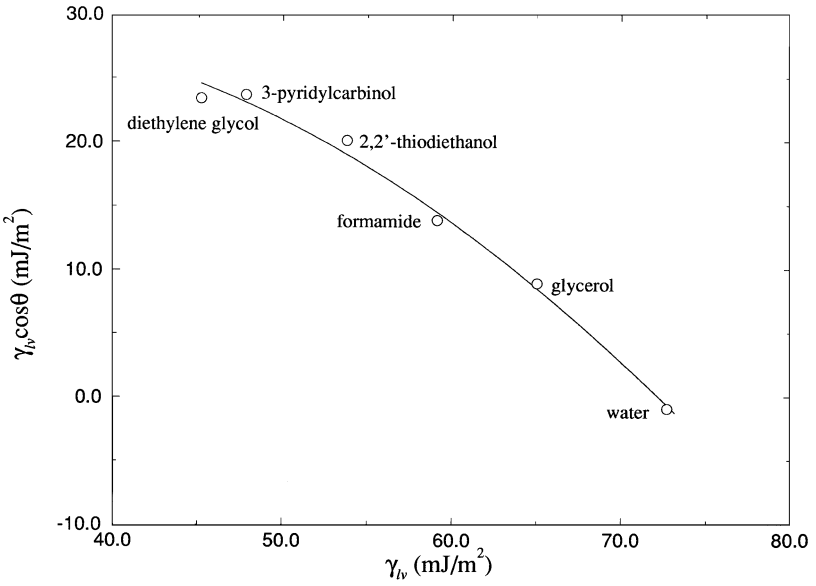

Fig. 3 The values of $\gamma_{lv}\cos\theta$ vs. γ_{lv} for the P*n*BMA-coated wafer surface, for the data in Table 2. Since the values of $\gamma_{lv}\cos\theta$ change smoothly with γ_{lv} at constant γ_{sv}, γ_{sl} can be expressed as a function of only γ_{lv} and γ_{sv} because of Young's equation

stipulate that γ_{sl} depends not only on γ_{lv} and γ_{sv}, but also on the specific intermolecular forces of the liquids and solids. But the above experimental results allow one to search for a relation in the form of Eq. (4).

On phenomenological grounds, an equation-of-state approach for solid–liquid interfacial tension has been formulated [14]:

$$\gamma_{sl} = \gamma_{lv} + \gamma_{sv} - 2\sqrt{\gamma_{lv}\gamma_{sv}}\, e^{-\beta(\gamma_{lv}-\gamma_{sv})^2}, \tag{5}$$

where β is a constant which was found to be $0.0001247\,(m^2/mJ)^2$. Combining this equation with Young's equation yields

$$\cos\theta_Y = -1 + 2\sqrt{\frac{\gamma_{sv}}{\gamma_{lv}}}\, e^{-\beta(\gamma_{lv}-\gamma_{sv})^2}. \tag{6}$$

Thus, the solid surface tensions can be determined from experimental (Young) contact angles and liquid surface tensions.

The applicability of any approach having the form of Eq. (4) can be tested using the criteria of the constancy of the calculated γ_{sv} values. Relations of the form of Eq. (4) have been in the literature for a long time. Two examples are Antonow's rule [48]

$$\gamma_{sl} = |\gamma_{lv} - \gamma_{sv}| \tag{7}$$

and Berthelot's geometric mean relationship [49]

$$\gamma_{sl} = \gamma_{lv} + \gamma_{sv} - 2\sqrt{\gamma_{lv}\gamma_{sv}}. \tag{8}$$

Combining these or similar relationships with Young's equation yields a relation of the form of Eq. (3), from which γ_{sv} can be calculated. We show in Table 4 the γ_{sv} values calculated from Antonow's rule [48], Berthelot's rule [49], and the equation-of-state approach for solid–liquid interfacial tensions [14], i.e. Eq. (6); the underlying Eq. (5) can be understood as a modified Berthelot rule [50]. It can be seen that the values of γ_{sv} calculated from Antonow's rule increase as γ_{lv} increases; the γ_{sv} values calculated from Berthelot's rule decrease as γ_{lv} increases. Only the γ_{sv} values from the equation-of-state approach for solid–liquid interfacial tensions are quite constant, essentially independent of the liquids used: the γ_{sv} value of P*n*BMA was found to be $28.81\,mJ/m^2$ with a 95% confidence limit of $\pm 0.54\,mJ/m^2$.

It should be noted that the constant β value of $0.0001247\,(m^2/mJ)^2$ used in the above calculations had been obtained only from contact angle data on three well-prepared solid surfaces [45]: FC-721-coated mica, heat-pressed Teflon (FEP), and poly(ethylene terephthalate) (PET). Alternatively, the γ_{sv} value of P*n*BMA can be determined by a two-variable least-square analysis [14], by assuming γ_{sv} and β in Eq. (6) to be constant. In this procedure, the computer will search for that pair of γ_{sv} and β values which provides the best fit of Eq. (6) to the six pairs of experimental (θ_Y, γ_{lv}) data points. This leads to a β value of $0.0001238\,(m^2/mJ)^2$ and a γ_{sv} value of $28.78\,mJ/m^2$. It is evident that there is good agreement between the γ_{sv} values ($28.81 \pm 0.54\,mJ/m^2$ and $28.78\,mJ/m^2$) as well as the β values determined from the two strategies. Using $\beta = 0.0001238\,(m^2/mJ)^2$ instead of $\beta = 0.0001247\,(m^2/mJ)^2$ yields virtually identical results for γ_{sv}.

The above results reconfirm the validity of the equation-of-state approach [14] to determine solid surface tensions from contact angles.

Table 4 The solid–vapor surface tension values γ_{sv} of a poly(*n*-butyl methacrylate) (P*n*BMA)-coated silicon wafer surface calculated from Antonow's rule [48], Berthelot's rule [49] and the equation of state approach for solid–liquid interfacial tensions [14]

Liquids	γ_{lv} [mJ/m^2]	θ [deg.]	γ_{sv} [mJ/m^2]		
			Antonow's rule	Berthelot's rule	Equation-of-state
Diethylene glycol	45.16	58.73 ± 0.64	34.30	26.05	28.03
3-Pyridylcarbinol	47.81	60.30 ± 0.25	35.75	26.73	29.16
2,2′-Thiodiethanol	53.77	68.00 ± 0.23	36.96	25.40	29.44
Formamide	59.08	76.41 ± 0.41	36.48	22.53	28.46
Glycerol	65.02	82.11 ± 0.21	36.97	21.02	29.04
Water	72.70	90.73 ± 0.79	35.89	17.71	28.71

Conclusions

(1) The values of $\gamma_{lv}\cos\theta$ change smoothly with γ_{lv}, in excellent agreement with those from other polar and non-polar surfaces [34–37, 45–47].

(2) The γ_{sv} values of P*n*BMA calculated from the equation-of-state approach [14] are quite constant, essentially independent of the liquids used; the average value is $\gamma_{sv} = 28.8 \pm 0.5\,\mathrm{mJ/m^2}$. This reconfirms the soundness of the approach to calculate solid surface tensions from contact angles.

Acknowledgements This research was supported by the Natural Science and Engineering Research Council of Canada (Grants: No. A8278 and No. EQP173469), Ontario Graduate Scholarships (D.Y.K.), and University of Toronto Open Fellowships (D.Y.K.).

References

1. Derjaguin BV, Muller VM, Toporov YP (1980) J Colloid Interface Sci 73:293
2. Johnson KL, Kendall K, Roberts AD (1971) Proc Roy Soc London A324:301
3. Muller VM, Yushchenko VS, Derjaguin BV (1983) J Colloid Interface Sci 92:92
4. Fogden A, White LR (1990) J Colloid Interface Sci 138:414
5. Pashley RM, McGuiggan PM, Horn RG, Ninham BW (1988) J Colloid Interface Sci 126:569
6. Christenson HK (1986) J Phys Chem 90:4
7. Claesson PM, Blom CE, Horn PC, Ninham BW (1986) J Colloid Interface Sci 114:234
8. Pashley PM, McGuiggan PM, Pashley RM (1987) Colloids Surf 27:277
9. Pashley RM, McGuiggan PM, Ninham BW, Evans DF (1985) Science 229:1088
10. Zisman WA (1964) Contact Angle, Wettability and Adhesion. In: Advances in Chemistry Series, Vol 43. American Chemical Society, Washington DC
11. Fowkes FM (1964) Ind Eng Chem 12:40
12. Driedger O, Neumann AW, Sell PJ, (1965) Kolloid-Z. Z Polym 201:52
13. Neumann AW, Good RJ, Hope CJ, Sejpal M (1974) J Colloid Interface Sci 49:291
14. Spelt JK, Li D (1996) The equation of state approach to interfacial tensions. In: Neumann AW, Spelt JK (eds) Applied Surface Thermodynamics. Marcel Dekker, New York, pp 239–292
15. Owens DK, Wendt RC (1969) J Appl Polym Sci 13:1741
16. van Oss CJ, Chaudhury MK, Good RJ (1988) Chem Revs 88:927
17. Good RJ, van Oss CJ (1992) The modern theory of contact angles and the hydrogen bond components of surface energies. In: Schrader M, Loeb G (eds) Modern Approaches to Wettability: Theory and Applications. Plenum Press, New York, pp 1–27
18. Bruil HG (1974) Colloid Polym Sci 252:32
19. Cheever GD (1983) J Coat Technol 55:53
20. Kilau HW (1983) Colloids Surf 26:217
21. Grundke K, Bogumil T, Gietzelt T, Jacobasch H-J, Kwok DY, Neumann AW (1996) Progr Colloid Polym Sci 101:58
22. Vargha-Butler EI, Zubovits TK, Absolom DR, Neumann AW (1985) Dispersion Sci Technol 6(3):357
23. Vargha-Butler EI, Moy E, Neumann AW (1987) Colloids Surf 24:315
24. Vargha-Butler EI, Zubovits TK, Absolom DR, Neumann AW (1985) Chem Eng Commun 33:255
25. Li D, Neumann AW (1996) Wettability and surface tension of particles. In: Neumann AW, Spelt JK (eds) Applied Surface Thermodynamics. Marcel Dekker, New York, pp 509–556
26. Omenyi SN, Neumann AW (1976) J Appl Phys 47:3956
27. Li D, Neumann AW (1996) Behavior of particles at solidification fronts. In: Neumann AW, Spelt JK (eds) Applied Surface Thermodynamics. Marcel Dekker, New York, pp 557–628
28. Moy E, Neumann AW (1996) Theoretical approaches for estimating solid–liquid interfacial tensions. In: Neumann AW, Spelt JK (eds) Applied Surface Thermodynamics. Marcel Dekker, New York, pp 333–378
29. van Giessen AE, Bukman DJ, Widom B (1997) J Colloid Interface Sci 192:257
30. Neumann AW (1974) Adv Colloid Interface Sci 4:105
31. Marmur A (1996) Colloids Surf A 116:25
32. Li D, Neumann AW (1996) Thermodynamic status of contact angles. In: Neumann AW, Spelt JK (eds) Applied Surface Thermodynamics. Marcel Dekker, New York, pp 109–168

33. Kwok DY, Li D, Neumann AW (1996) Capillary rise at a vertical plate as a contact angle technique. In: Neumann AW, Spelt JK (eds) Applied Surface Thermodynamics. Marcel Dekker, New York, pp 413–440
34. Kwok DY, Budziak CJ, Neumann AW (1995) J Colloid Interface Sci 173:143
35. Kwok DY, Lin R, Mui M, Neumann AW (1996) Colloids Surf A 116:63
36. Kwok DY, Gietzelt T, Grundke K, Jacobasch H-J, Neumann AW (1997) Langmuir 13:2880
37. del Rio OI, Kwok DY, Wu R, Alvarez JM, Neumann AW, Colloids Surf A, accepted for publication
38. Oliver JF, Huh C, Mason SG (1977) J Colloid Interface Sci 59:568
39. Oliver JF, Huh C, Mason SG (1980) Colloids Surf 1:79
40. Rotenberg Y, Boruvka L, Neumann AW (1983) J Colloid Interface Sci 93:169
41. Cheng P, Li D, Boruvka L, Rotenberg Y, Neumann AW (1983) Colloids Surf 93:169
42. Lahooti S, del Rio OI, Cheng P, Neumann AW (1996) Axisymmetric drop shape analysis. In: Neumann AW, Spelt JK (eds) Applied Surface Thermodynamics. Marcel Dekker, New York, pp 441–507
43. Duncan D, Li D, Gaydos J, Neumann AW (1995) J Colloid Interface Sci 169:256
44. Gaydos J, Neumann AW (1996) Line tension in multiphase equilibrium systems. In: Neumann AW, Spelt JK (eds) Applied Surface Thermodynamics. Marcel Dekker, New York, pp 169–238
45. Li D, Neumann AW (1992) J Colloid Interface Sci 148:190
46. Li D, Xie M, Neumann AW (1993) Colloid Polym Sci 271:573
47. Kwok DY, Li D, Neumann AW (1994) Colloids Surf A 89:181
48. Antonow G (1907) J Chim Phys 5:372
49. Berthelot D (1898) Compt rend 126, 1703:1857
50. Li D, Neumann AW (1990) J Colloid Interface Sci 137:304